Analysis and Design of a Partial-Power Post-Regulator Based DC/DC Converter for Automotive Applications

Nicola Zanatta*, Tommaso Caldognetto*, Davide Biadene*, Giorgio Spiazzi†, and Paolo Mattavelli*

*Department of Management and Engineering, University of Padova, Vicenza, Italy
†Department of Information Engineering, University of Padova, Padova, Italy
nicola.zanatta.2@phd.unipd.it, tommaso.caldognetto@unipd.it, davide.biadene@unipd.it, giorgio.spiazzi@unipd.it, paolo.mattavelli@unipd.it

***Abstract*—This paper proposes and analyzes a partial-power (PP) converter for electric vehicle charging applications, where high efficiency over a wide range of battery voltages is required. The proposed converter employs a first dual-output isolation stage and a second dual-input buck post-regulator. In such a post-regulator, only a fraction of the transferred power is processed, whereas the other part of the output power flows directly to the load without any conversion losses. This allows high efficiency even with output voltages that may vary over a wide range. The isolation stage is always operated at resonance, it behaves as a dual-output dc-transformer (DCX), ensuring very high efficiency. The conversion structure, analysis, and design considerations are shown considering a prototype rated 10 kW and interfacing a 800 V dc-link with an output bus in the voltage range 250 V - 500 V, which is common in electric vehicle battery-charging applications.**

***Index Terms*—battery charger, dc-dc converter, dual-input buck converter, DCX, fast-charging, resonant LLC, post-regulation, soft-switching.**

I. Introduction

The electric transportation model is gaining ground in many countries due to growing concerns about global greenhouse gas emissions and fossil fuel depletion [1], [2]. DC-DC converters with galvanic isolation are the beating heart of an effective electric-vehicle (EV) battery charging systems [3]–[6]. The resonant LLC converter is commonly adopted in many applications for its simple structure and efficient power conversion, thanks to its inherent zero-voltage switching (ZVS) and zero-current switching (ZCS) operation for primary-side and secondary-side switches, respectively. However, performance significantly degrades at input or output voltages that do not allow near-resonance operation [4], [7]. This is often the case in the considered application, represented in Fig. 1, where battery state of charge variations due to typical mission profiles may bring to wide ranges of operating voltages [2], [4], [8], [9]. An effective method to overcome the limitations of the frequency-modulated LLC converter is to keep working the LLC stage in its optimal operating point (i.e. DCX operation) and employ an additional partial-power (PP) stage to regulate the output voltage [5], [10]–[13]. This PP converter provides the possibility to process only a fraction of the rated power of the resonant converter, while the remainder of the input power is transferred directly to the load, with no conversion loss [11], [13]. Hence, the losses of the post-processing stage have only a marginal impact on the overall efficiency of the converter, even when working with a wide range of input or output voltages. Partial-power conversion solutions show potential advantages to accommodate wide operating voltage ranges for applications like in Fig. 1, at the cost of a higher number of components and a more complex design of DCXs stages, but advantageous characteristics in terms of overall conversion efficiency can be expected [10], [11].

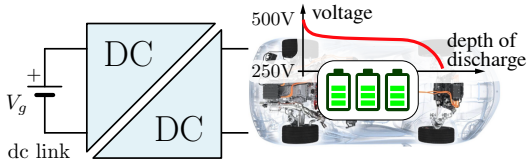

Fig. 1: EV-charging application.

In this paper, a DC/DC converter with partial-power post-regulator is proposed, analyzed, and evaluated by means of PLECS simulations. As shown in Fig. 2, the inputs of the PP regulator are directly connected to the LLC outputs provided by means of a three-winding transformer and subsequent rectifiers (i.e., V_1 and V_2 ports respectively). The principle is to operate the main converter at the operating condition that ensures maximum efficiency, namely, at resonance, and exploit the post-regulation stage working at lower voltage stress to perform the output voltage regulation. Despite of the presence of an additional stage respect to a full-power processing approach (i.e., a LLC stage followed by a buck converter), the output power is processed by the post-regulator

This work has been created in the context of the PROGRESSUS project. This project has received funding from the Electronic Components and Systems for European Leadership Joint Undertaking under grant agreement No 876868. This Joint Undertaking receives support from the European Unions Horizon 2020 research and innovation program and Germany, Slovakia, Netherlands, Spain, Italy.

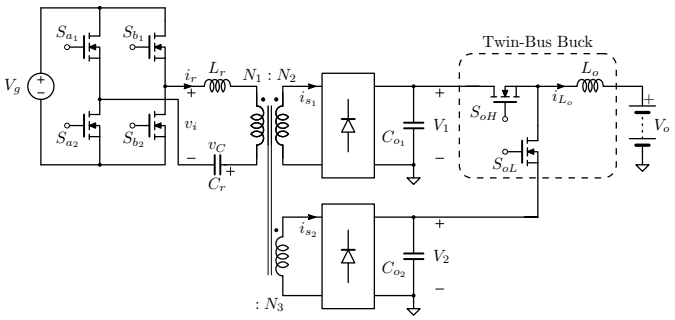

Fig. 2: Proposed Partial-Power based converter scheme implementation.

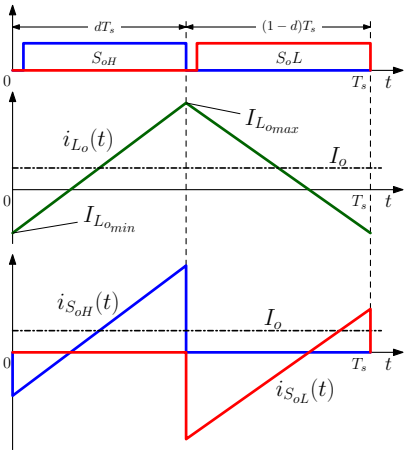

Fig. 3: Main waveforms of TBB stage shown in Fig. 2. In order: gate driver signals including dead times, L_o inductor current and $S_{1,2}$ switch currents.

in function of the output voltage, sharing the power among the two PP-stage inputs and therefore potential efficiency advantages can be reached. The merits of the solution and the related efficiency improvements are described in this work.

In the following, the topology is introduced in Sect. II. The DCX stage design is discussed in Sect. III and some simulation results are reported in Sect. IV. Conclusions are reported in Sect. V.

II. Converter Structure and Operation

A. Partial-Power Converter Configuration

Different configurations of DC/DC converters exploiting partial-power concept have been examined and proposed in the literature [5], [10], [13]. As shown in Fig. 2, the proposed converter consists of a first isolation stage based on a LLC resonant converter, and a partial-power rated converter parallel-connected with the load. Such a post regulator is responsible of the output voltage regulation and it is supplied by means of a high efficiency dual-output DCX converter. From Fig. 2, it is clear that the voltage stress of the post-regulator can be lower that the output voltage V_o, which consequently lead to smaller on-resistance of the semiconductors as well as smaller switching losses.

It is worth remarking that the topology where the two DCX-LLC outputs are connected in series can also be considered. This variant will be considered in future investigations. Preliminary studies, shown as potential advantage in the transformer design.

B. Partial-Power Post-Regulator and Main Waveforms

The dual-input partial-power rated DC/DC regulator is shown in Fig. 2 while its main waveforms are shown in Fig. 3. It is based on a simple dual-input buck topology [14], herein referred to as Twin-Bus Buck (TBB) converter, designed to operate in Quasi-Square Wave, i.e, with a peak-to-peak inductor current ripple higher than twice the average load current. This allows the Zero Voltage turn on of both switches, S_{oH} and S_{oL}. The TBB is responsible of the output voltage regulation of the whole converter. The output voltage V_o is a function of the input voltages of the TBB, V_1 and V_2 with $V_1 > V_2$, and the duty cycle of the upper switch (i.e, S_{oH}), namely d:

$$V_o = d\,V_1 + (1-d)\,V_2 \tag{1}$$

For fixed input voltages V_1 and V_2, the minimum and maximum output voltages can be defined as:

$$\begin{aligned} V_{o_{min}} &= d_{min}\,V_1 + (1-d_{min})\,V_2 \\ V_{o_{max}} &= d_{max}\,V_1 + (1-d_{max})\,V_2 \end{aligned} \tag{2}$$

with d_{min} and d_{max} the minimum and maximum duty cycles of S_{oH}, referred to $V_{o_{min}}$ and $V_{o_{max}}$ respectively. Their value must guarantee the zero-voltage switching operation of S_{oH} and S_{oL} at correspondent output voltage levels. Thus the needed input voltages V_1 and V_2 provided by the DCX stage, can be calculated from (2) as:

$$\begin{aligned} V_1 &= \frac{V_{o_{max}}(1-d_{min}) - V_{o_{min}}(1-d_{max})}{d_{max}-d_{min}} \\ V_2 &= \frac{V_{o_{min}}d_{max} - V_{o_{max}}d_{min}}{d_{max}-d_{min}} \end{aligned} \tag{3}$$

The maximum voltage stress of the switches, $V_1 - V_2$, can be derived from (3) as:

$$V_1 - V_2 = \frac{V_{o_{max}} - V_{o_{min}}}{d_{max}-d_{min}} \tag{4}$$

that is always lower than the voltage stress of the switches of a full-power converter that requires a supply voltage higher than the maximum output voltage. The output power is shared among both inputs of the TBB in function of the output voltage. Starting from (1) and (3), the normalized input powers Π_i, with $i = 1, 2$, at the i-th port of TBB are:

$$\begin{aligned} \Pi_1 &= \frac{V_1}{V_1 - V_2} - \frac{V_1 V_2}{V_1 - V_2}\cdot\frac{1}{V_o} \\ \Pi_2 &= -\frac{V_2}{V_1 - V_2} + \frac{V_1 V_2}{V_1 - V_2}\cdot\frac{1}{V_o} \end{aligned} \tag{5}$$

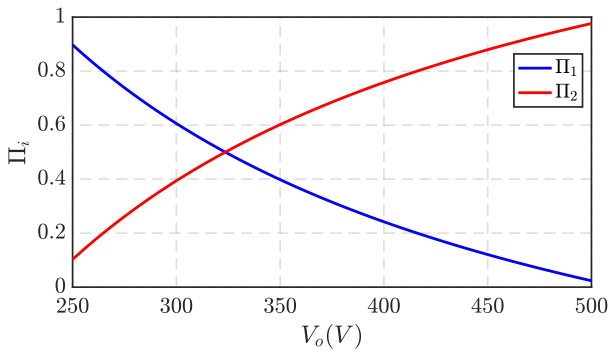

Fig. 4: Power allocation on TBB based on converter scheme implementing Fig. 2.

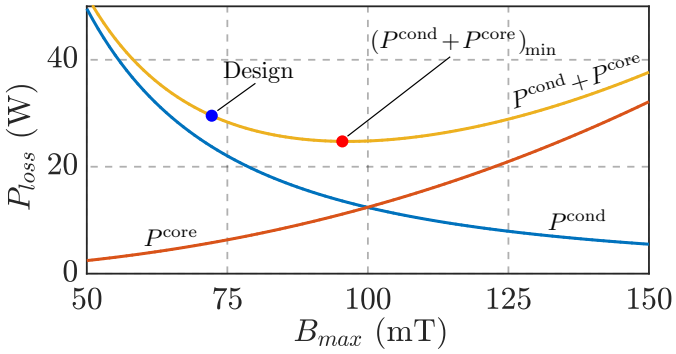

Fig. 5: P-B plot for transformer design at $V_o = 400\,\text{V}$ and $P_o = 10\,\text{kW}$.

where the normalization is done respect to the output power $P_o = V_o I_o$.

For instance, by imposing $d_{min} = (1 - d_{max}) = 5\%$, the power allocation done by the TBB in function of output voltage is reported in Fig. 4. A 5% of duty cycle with a reduced switching frequency allows to achieve ZVS for the whole output voltage range with a proper selection of the output inductor value. Therefore, MOSFETs with low on-resistance allow to increase the converter efficiency [10], [11].

III. Design of LLC Stage Operated as DCX

The converter structure is shown in Fig. 2. When the LLC resonant tank is operated exactly at its resonance frequency, the voltage conversion ratio becomes ideally independent from the actual load. In other words, the LLC converter maintains a constant voltage conversion ratio and adjusts its current automatically, according to the load conditions, behaving as a DC-transformer (DCX). In this operating condition the LLC shows its maximum efficiency, indeed additional reactive power is not processed and zero-voltage switching and zero-current switching conditions are always satisfied [11]. The transformer turns ratio can be calculated as $n_1 = N_2/N_1 = 0.642$ and $n_2 = N_3/N_1 = 0.295$ to make the LLC converter operate at the resonant frequency f_s at input voltage $V_g = 800\,\text{V}$ and output voltages range V_2 - V_1.

A. Transformer Design

In the design of the main magnetic element, both winding and core losses must be considered. The transformer design procedure adopted herein is based on [15], [16].

Once the magnetic core is selected, with given magnetic volume V_c, window winding area W_a, core cross-sectional area A_c, Steinmetz parameters K_c, α and β, and maximum window filling factor k_u (typ., assume $k_u \leq 40\%$), it is possible to calculate the winding losses, P^{cond}, as:

$$P^{\text{cond}} = RF(f_s)\rho_w V_w k_u J_0^2 \tag{6}$$

where ρ_w is the copper resistivity, V_w is the total windings volume, $RF(f_s) = R^{\text{ac}}/R^{\text{dc}}$ is the resistivity factor for the selected litz wire at fundamental frequency [15] and J_0 is the current density. The last parameter is calculated as:

$$J_0 = \frac{\sum VA}{K_v f_s k_f B_{max} k_u A_p} \tag{7}$$

with $\sum VA$ is the power rating of the transformer, K_v is the waveform factor, f_s is the fundamental frequency, B_{max} is the peak flux density, k_f is core stacking factor, and $A_p = A_c W_a$ is the area product of the core.

The core losses, P^{core}, can be estimated using the Steinmetz equation:

$$P^{\text{core}} = V_c K_c f_s^{\alpha} B_{max}^{\beta} \tag{8}$$

where K_c, α and β are the Steinmetz parameters for the considered material, while V_c is the core volume. The total transformer dissipated power is then computed as the sum of (6) and (8) and it must be lower than the thermal dissipation capability of the component, which can be estimated during the design phase. Fig. 5 reports the results of the calculated transformer losses, showing a total loss of 24 W at nominal conditions, namely, $V_1 = 514\,\text{V}$ and $V_2 = 236\,\text{V}$, and $P_o = 10\,\text{kW}$. According with Fig. 5, the selected design point is more conservative in terms of core losses respect the optimal point, this is due to a trade-off between the desired magnetizing inductance and the conductor sections. The designed transformer has turns ratio $n_1 = 0.625$ and $n_2 = 0.292$, current density $J_0 = 5\,\text{A/mm}^2$, number of turns per winding $N_1 = 24$, $N_2 = 15$, $N_3 = 7$.

B. Resonant Tank Design

For what concerns the design of the resonant $L_r C_r$ tank, the transformer leakage inductance can be exploited for the implementation of the inductive part. Given the DCX operation mode of the LLC, low values of L_m can be used, which is beneficial in terms of transformer design, losses, and resonant capacitor voltage stress. With the aimed DCX operation, the value of the magnetizing inductance L_m is typically chosen to ensure a sufficiently high magnetizing current to allow ZVS for all the switches of the main converter. A classical design for a DCX-LLC with voltage ratings of Table I (refer, for example, to [11]) requires a magnetizing inductance of about 200 µH.

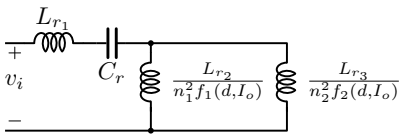

Fig. 6: Equivalent resonant tank of Fig. 2.

The designed transformer achieves the project target, with a magnetizing inductance of about 215 µH. The capacitive part of the resonant tank can be selected on the basis of the desired resonant frequency (i.e., converter switching frequency given the DCX LLC operation). The experimental prototype shows values of leakage inductances of $L_{r_1} = 795\,\text{nH}$, $L_{r_2} = 445\,\text{nH}$, and $L_{r_3} = 271\,\text{nH}$, for the design in Fig. 5. The secondary windings leakage inductances L_{r_2} and L_{r_3} affect the overall resonance frequency proportionally to the normalized conduction interval of the respective diode bridge rectifier. In fact, these inductances come into play only when the corresponding rectifier diodes are conducting, and these intervals are related to the duty-cycle of the TBB stage, as well as to the load current. For these reasons, the equivalent resonant tank of Fig. 6 includes these inductances weighted by functions $f_1(d, Io)$ and $f_2(d, Io)$, whose values are less than one, and dependent on the converter operating point. Remarkably, the equivalent inductances referred to the primary side are function of the duty cycle d and the output current I_o, therefore also function of the output voltage, according to (1). This gives a value of series-equivalent inductance of the resonant L_rC_r tank of:

$$L_r(d, I_o) = L_{r_1} + \frac{L_{r_2}L_{r_3}}{L_{r_2}n_2^2 f_2(d, I_o) + L_{r_3}n_1^2 f_1(d, I_o)} \quad (9)$$

that is function of the converter operating point. In order to remove the dependence of the resonance frequency from the load, two additional resonant capacitors are connected in series with the two output ports of the transformer, as shown in Fig. 7. At resonance, the capacitive part of each of the series-resonant impedances $L_{r_i}C_{r_i}$ cancels out with the corresponding inductive part. $C_{r_1} = 796\,\text{nF}$, $C_{r_2} = 1.42\,\mu\text{F}$ and $C_{r_3} = 2.34\,\mu\text{F}$ are then calculated as proper values for the resonant capacitances in order to achieve a continuous resonant current operation, where the resonant frequency of LLC stage becomes independent of duty-cycle and output current of TBB stage, as otherwise showed in (9). The proposed PP post-regulated converter is shown in Fig. 7.

IV. Simulation Results

A converter topology with parameters reported in Table I is considered for validation. Based on the considerations reported in Sect. III, herein are reported the simulation results focused on demonstrating the continuous resonant current operation of the DCX stage. First, the operation of the converter in Fig. 2 is considered with a single resonant capacitor C_r and, then, the operation of the proposed converter in Fig. 7 is considered. Converters in Fig. 2 and Fig. 7 are simulated and the resonant currents are shown in Fig. 8. Let us consider different operating

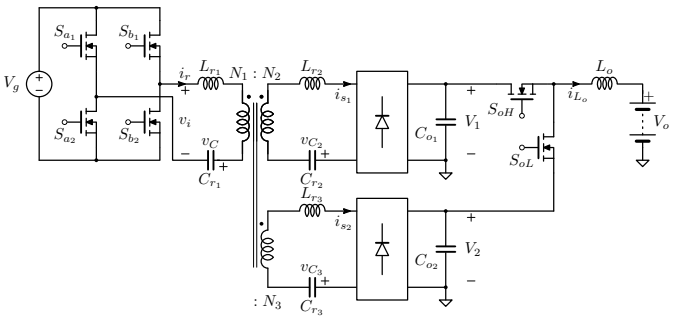

Fig. 7: DCX-LCC + Twin-Bus Buck converter scheme.

TABLE I: Converter parameters.

Parameter	Symbol	Value	
Input voltage	V_g	800	V
Minimum output voltage	$V_{o_{min}}$	250	V
Maximum output voltage	$V_{o_{max}}$	500	V
Nominal power	P_o^{nom}	10	kW
Switching frequency	f_s	200	kHz
Turns ratio N_2/N_1	n_1	0.625	-
Turns ratio N_3/N_1	n_2	0.292	-
Magnetizing inductance	L_m	215	µH
Leakage inductances	L_{r_1}	795	nH
	L_{r_2}	445	nH
	L_{r_3}	271	nH
Resonant capacitances	C_{r_1}	796	nF
	C_{r_2}	1.42	µF
	C_{r_3}	2.34	µF
S_{a_1,a_2,b_1,b_2}	G3R30MT12K, SiC MOSFETs		
S_{oH}, S_{oL}	GPI65060DFN, GaN HEMTs		
Output Rectifiers	C5D50065D, SiC diodes		

points at $I_o = 25\,\text{A}$ and $V_o = 250, 400, 500\,\text{V}$. Figs. 8(a)-(c) shows the resonant currents i_r,i_{s_1} and i_{s_2}, and the magnetizing current i_m of the circuit in Fig. 2 with resonant capacitance $C_r = 174\,\text{nF}$. Such value is properly designed to have the desired resonance frequency f_s, with $L_r = 3.64\,\mu\text{H}$ given by (9) at $V_o = 250\,\text{V}$. While, Figs. 8(d)-(f) shows the resonant currents considering the circuit in Fig. 7 with resonant capacitances C_{r_i} of Table I. From the simulation results it is clear to see that the resonance conditions are satisfied only for this later case, for the whole wide output voltage range. Furthermore, conduction losses are minimized only if the resonance conditions are satisfied. In Fig. 9 are reported and compared the efficiency performances of the proposed topology, a full-bridge LLC and the topology in [16], for $V_o = 250\,\text{V}$, $400\,\text{V}$ and $500\,\text{V}$. Such a simulation results are obtained through PLECS models and they include accurate loss models of switching, magnetic and conduction losses. Compared with the considered solutions, from Fig. 9 is possible to see that the proposed topology can offer prominent

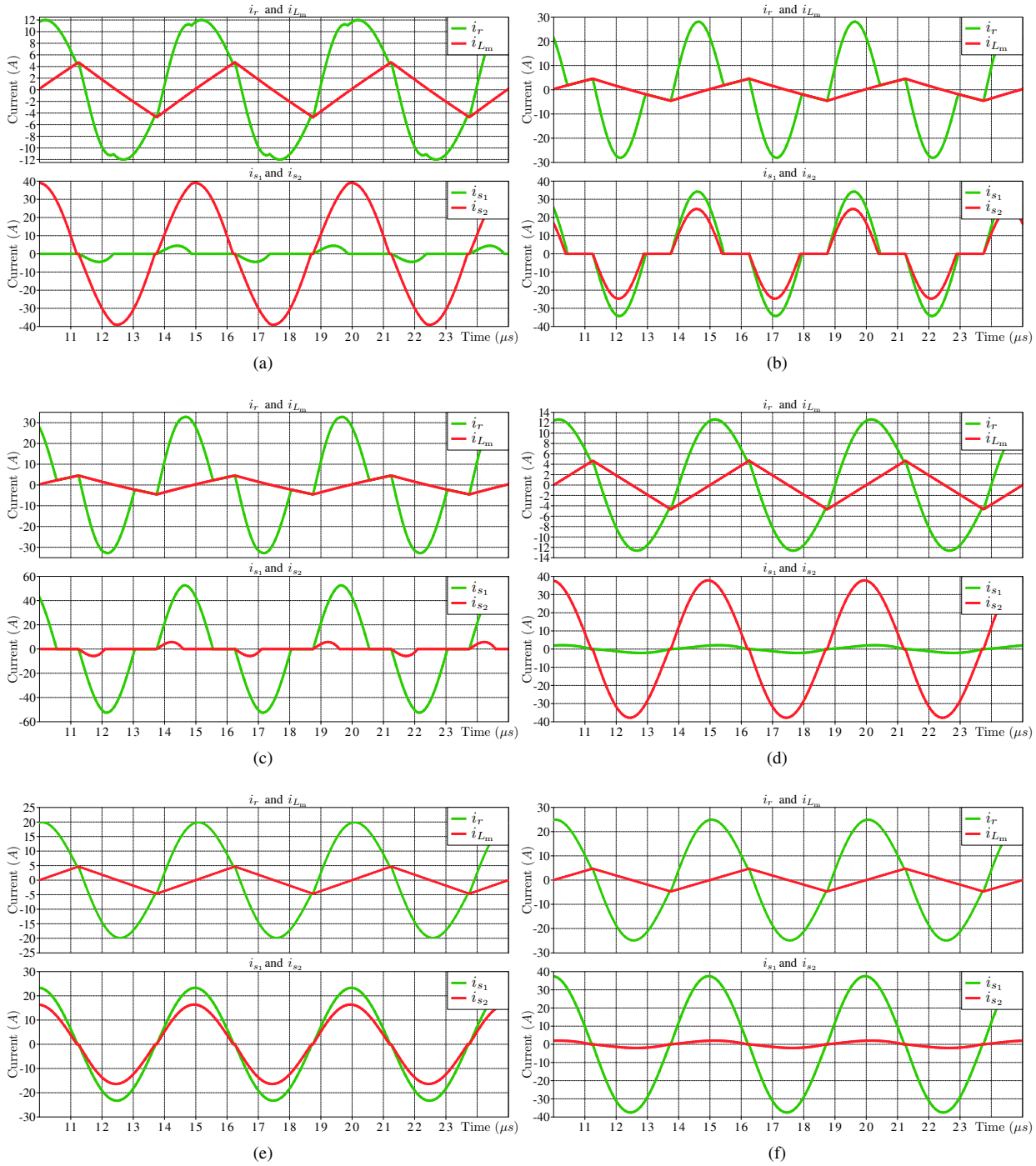

Fig. 8: Simulation results for LLC with different resonant tank designs, (a)-(c) refer to Fig. 2 and (d)-(f) refer to Fig. 7. (a),(d) $V_o = 250\,\mathrm{V}$; (b),(e) $V_o = 400\,\mathrm{V}$; (c),(f) $V_o = 500\,\mathrm{V}$. Converter parameters are reported in Table I.

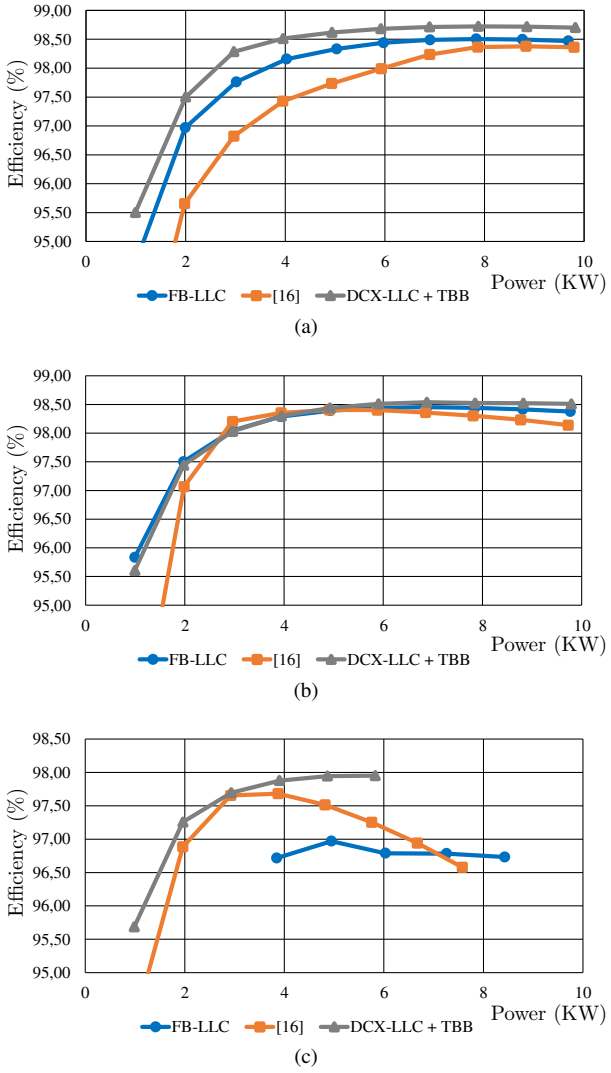

Fig. 9: Efficiency comparison: full-bridge LLC, topology proposed in [16], and proposed topology. (a) $V_o = 500\,\mathrm{V}$, (b) $V_o = 400\,\mathrm{V}$ and (c) $V_o = 250\,\mathrm{V}$.

efficiency improvements, at the cost of a small component increment.

V. Conclusions

The work analyzes a partial-power converter composed of a DCX-LLC and a post-regulator for battery charging applications. The LLC converter always operates at its optimal operating point and the additional PP converter based on a dual-input buck converter is used to regulate the output voltage. Hence, the efficiency and the volume of the proposed configuration, compared with standard DC/DC converters processing full power, can be improved. The considered topology is presented, simulation results of a resonant dual-output LLC are reported and an efficiency performances comparison considering $10\,\mathrm{kW}$ topologies is included.

References

[1] *Global EV Outlook 2021*, International Energy Agency, 2021. [Online]. Available: https://www.iea.org/reports/global-ev-outlook-2021

[2] S. Rivera, S. Kouro, S. Vazquez, S. M. Goetz, R. Lizana, and E. Romero-Cadaval, "Electric vehicle charging infrastructure: From grid to battery," *IEEE Industrial Electronics Magazine*, vol. 15, no. 2, pp. 37–51, jun 2021.

[3] D. Ronanki, A. Kelkar, and S. S. Williamson, "Extreme fast charging technology—prospects to enhance sustainable electric transportation," *Energies*, vol. 12, no. 19, p. 3721, sep 2019.

[4] H. Tu, H. Feng, S. Srdic, and S. Lukic, "Extreme fast charging of electric vehicles: A technology overview," *IEEE Transactions on Transportation Electrification*, vol. 5, no. 4, pp. 861–878, dec 2019.

[5] V. M. Iyer, S. Gulur, G. Gohil, and S. Bhattacharya, "An approach towards extreme fast charging station power delivery for electric vehicles with partial power processing," *IEEE Transactions on Industrial Electronics*, vol. 67, no. 10, pp. 8076–8087, oct 2020.

[6] T. Blank, B. An, D. Bauer, P. Jochem, M. Luh, H. Wurst, and M. Weber, "Highly integrated sic-power modules for ultra-fast lithium-ionbattery chargers in llc-topology," in *PCIM Europe 2018; International Exhibition and Conference forPower Electronics, Intelligent Motion, Renewable Energy and Energy Management*. Stuttgart, Germany: Mesago Messe Frankfurt GmbH, 2018, pp. 1–8.

[7] Y. Hu, J. Shao, and T. S. Ong, "6.6 kW high-frequency full-bridge LLC DC/DC converter with SiC MOSFETs," in *2019 IEEE Energy Conversion Congress and Exposition (ECCE)*. IEEE, sep 2019.

[8] Q. Cao, Z. Li, and H. Wang, "Wide voltage gain range LLC DC/DC topologies: State-of-the-art," in *2018 International Power Electronics Conference (IPEC-Niigata 2018 -ECCE Asia)*. IEEE, may 2018.

[9] Z. Li, B. Xue, and H. Wang, "An interleaved secondary-side modulated LLC resonant converter for wide output range applications," *IEEE Transactions on Industrial Electronics*, vol. 67, no. 2, pp. 1124–1135, feb 2020.

[10] Y. Cao, M. Ngo, N. Yan, D. Dong, R. Burgos, and A. Ismail, "Design and implementation of an 18 kW 500 kHz 98.8% efficiency high-density battery charger with partial power processing," *IEEE Journal of Emerging and Selected Topics in Power Electronics*, pp. 1–1, 2021.

[11] D. Neumayr, M. Vohringer, N. Chrysogelos, G. Deboy, and J. W. Kolar, "P^{3}DCT—Partial-Power Pre-Regulated DC Transformer," *IEEE Transactions on Power Electronics*, vol. 34, no. 7, pp. 6036–6047, jul 2019.

[12] L. Zhang, X. Wu, and H. Chen, "1mhz LLC resonant DC-DC converter with PWM output regulation capability," in *2016 IEEE 8th International Power Electronics and Motion Control Conference (IPEMC-ECCE Asia)*. IEEE, may 2016.

[13] I. Lopusina and P. Grbovic, "Comparative analysis of input-series-output-series partial power rated DC to DC converters," in *2021 21st International Symposium on Power Electronics (Ee)*. IEEE, oct 2021.

[14] J. Sebastian, P. Villegas, F. Nuno, and M. Hernando, "High-efficiency and wide-bandwidth performance obtainable from a two-input buck converter," *IEEE Transactions on Power Electronics*, vol. 13, no. 4, pp. 706–717, jul 1998.

[15] W. Wlfle and W. Hurley, *Transformers and Inductors for Power Electronics: Theory, Design and Applications*. Wiley, Apr. 2013.

[16] N. Zanatta, T. Caldognetto, G. Spiazzi, and P. Mattavelli, "A two-stage isolated resonant DC-DC converter for wide voltage range operation," in *2021 IEEE International Conference on Environment and Electrical Engineering and 2021 IEEE Industrial and Commercial Power Systems Europe (EEEIC / I&CPS Europe)*. IEEE, sep 2021.